

# VILA-M3: Enhancing Vision-Language Models with Medical Expert Knowledge

Vishwesh Nath<sup>1</sup>    Wenqi Li<sup>1</sup>    Dong Yang<sup>1</sup>    Andriy Myronenko<sup>1</sup>    Mingxin Zheng<sup>1</sup>  
 Yao Lu<sup>1</sup>    Zhijian Liu<sup>1</sup>    Hongxu Yin<sup>1</sup>    Yucheng Tang<sup>1</sup>    Pengfei Guo<sup>1</sup>    Can Zhao<sup>1</sup>  
 Ziyue Xu<sup>1</sup>    Yufan He<sup>1</sup>    Yee Man Law<sup>2</sup>    Benjamin Simon<sup>3</sup>    Stephanie Harmon<sup>3</sup>  
 Greg Heinrich<sup>1</sup>    Stephen Aylward<sup>1</sup>    Marc Edgar<sup>1</sup>    Michael Zephyr<sup>1</sup>    Song Han<sup>1</sup>  
 Pavlo Molchanov<sup>1</sup>    Baris Turkbey<sup>1</sup>    Holger Roth<sup>1,‡</sup>    Daguang Xu<sup>1,‡</sup>

<sup>1</sup>NVIDIA    <sup>2</sup>SingHealth    <sup>3</sup>NIH

<sup>‡</sup>Equal advisory

**Abstract:** Generalist vision language models (VLMs) have made significant strides in computer vision, but they fall short in specialized fields like healthcare, where expert knowledge is essential. Current large multimodal models like Gemini and GPT-4o are insufficient for medical tasks due to their reliance on memorized internet knowledge rather than the nuanced expertise required in healthcare. Meanwhile, existing medical VLMs (e.g. Med-Gemini) often lack expert consultation as part of their design, and many rely on outdated, static datasets that were not created with modern, large deep learning models in mind. VLMs are usually trained in three stages: vision pre-training, vision-language pre-training, and instruction fine-tuning (IFT). IFT has been typically applied using a mixture of generic and healthcare data. In contrast, we propose that for medical VLMs, a fourth stage of specialized IFT is necessary, which focuses on medical data and includes information from domain expert models. Domain expert models developed for medical use are crucial because they are specifically trained for certain clinical tasks, e.g. to detect tumors and classify abnormalities through segmentation and classification, which learn fine-grained features of medical data—features that are often too intricate for a VLM to capture effectively. This paper introduces a new framework, VILA-M3, for medical VLMs that utilizes domain knowledge via expert models. We argue that generic VLM architectures alone are not viable for real-world clinical applications and on-demand usage of domain-specialized expert model knowledge is critical for advancing AI in healthcare. Through our experiments, we show an improved state-of-the-art (SOTA) performance with an average improvement of  $\sim 9\%$  over the prior SOTA model Med-Gemini and  $\sim 6\%$  over models trained on the specific tasks. Our approach emphasizes the importance of domain expertise in creating precise, reliable VLMs for medical applications.

**Links:** [Code](#) (GitHub) | [Models](#) (Hugging Face) | [Demo](#)

## 1. Introduction

Large language models (LLMs) are at the forefront of AI. Recent works [1, 2] have enabled LLMs to support visual inputs to expand on their use for many vision applications by transforming them into vision language models (VLM). While foundational VLMs developed for computer vision applications have achieved remarkable success in various general-purpose tasks, they struggle to meet the necessary precision required for medical tasks [3, 4, 5]. VLMs trained on general tasks often lack specialized medical domain knowledge to interpret radiological images correctly [6, 5, 7]. VLMs without specific medical training also often miss the subtle visual details that are critical for medical diagnosis. For example, a recent study on breast imaging [8] shows that generic models like GPT-4o (OpenAI)

are not suitable for medical use cases. At the same time, there are healthcare-specific large VLMs such as Med-Gemini ( $\sim 1.5$  trillion parameters) [9], which are designed without consideration of expert model information and are likely to neglect finer visual features. Current VLMs are well-adapted to connect coarse or dominating visual features with language. However, they often fail to recognize finer visual details (Fig. 3). There are multiple reasons for these deficits. A major reason is the limited availability of comprehensive and clinically relevant public datasets for medical vision language tasks. Most public datasets in medical imaging were released to address specific narrow AI tasks like classification, regression, and segmentation [10]. At the same time, healthcare datasets incorporating natural language are limited to specific tasks such as visual question answering (VQA) and report generation, which

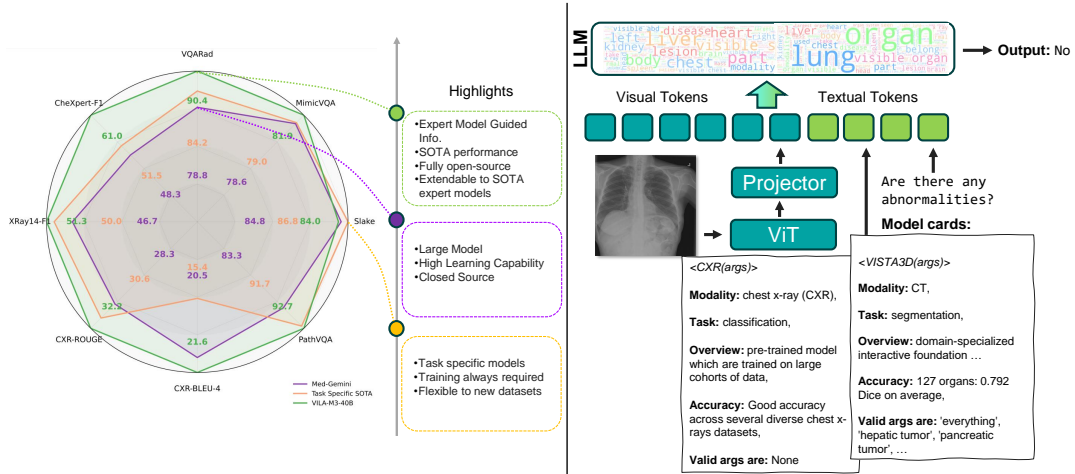


Figure 1 | Left: Comparison of VILA-M3 with SOTA benchmarks such as Med-Gemini and task-specific SOTA models. VILA-M3-40B performance is shown in comparison. It can be observed that VILA-M3 provides a generalizable better performance for all datasets. Right: VILA-M3 architecture overview, the model aligns visual features using a projection layer with textual user prompts and model cards describing available “expert models”.

do not cover the breadth of clinically relevant tasks.

Over the years, medical imaging has shown successful applications of specialized narrow AIs that solve specific medical imaging tasks, such as semantic segmentation. These “expert models” have already been incorporated into clinical workflows, such as pre-operative planning, patient triage, and more. Many have received regulatory approval (e.g., FDA) and, therefore, incorporating the “knowledge” of existing expert models into the decision-making and generation process of VLMs, specifically in healthcare, should markedly improve the overall performance on clinically relevant tasks.

In this work, we propose a new VLM framework, **VILA-M3**, that addresses the unique challenges faced by general-purpose VLMs when applied to the medical domain by incorporating the domain-expert knowledge of existing segmentation and classification models. We evaluate our approach on several medical imaging benchmarks and show significant improvements over the state of the art (SOTA), see Fig. 1.

### 1.1. Key challenges

Next, we summarize the key challenges that VILA-M3 aims to address.

#### Limitations of Existing Medical Datasets:

The majority of publicly available medical datasets used for model training and evaluation are static and not tailored for training for large VLMs [11, 12, 13, 14, 15, 16, 17]. The datasets were originally designed for earlier machine learning approaches, and they do not reflect the complexities required for

modern deep learning models such as VLMs. This need has sparked the generation of newer datasets such as [18, 19, 20]. In medicine, the constant need for expert validation and the evolving nature of healthcare data make static datasets insufficient for accurate model evaluation. In this work, we outline the need for more dynamic and adaptive approaches and show that on-demand usage of domain expert models can lead to improved model performance. The dataset limitation is one of the primary reasons we require and utilize expert model information in our framework. While large models like GPT-4o have been suggested as potential tools for evaluating model performance in medicine, their reliance on memorized information makes them unreliable for precision-critical tasks [6, 5].

#### Combining General Vision-Language Data with Healthcare Data:

Healthcare-specific datasets, while valuable, are not sufficient to fully train models that also require linguistic understanding. To overcome the aforementioned challenge, we utilize a four-stage training schema: pre-training vision encoder, pre-training VLM, instruction fine-tuning (IFT), and IFT with domain expert information. The two stages of IFT ensure that models can *preserve* their language capabilities without sacrificing performance on medical benchmarks [21]. This approach not only enhances their overall performance but also addresses the unique challenges posed by medical language and its precision requirements.

## 1.2. Contributions

Motivated by the above challenges, we present the following key contributions of our work:

- *Expert Knowledge Integration:* We emphasize the need for integrating expert knowledge into medical VLMs to improve precision.
- *Comprehensive capability:* VILA-M3 is the first medical VLM that can tackle segmentation, classification, report generation, and VQA tasks in one framework.
- *Expert-guided instruction fine-tuning:* We preserve the VLMs language capabilities by introducing expert-guided IFT training on top of the built VLM training schemes.
- *Hybrid 2D/3D Information Fusion:* We introduce effective integration with 2D and 3D expert models, enabling hybrid fusion of domain expert models that provide relevant 3D spatial information to enhance VLMs limited to 2D inputs.
- *Open-Source Module:* We provide an open-source module for data preparation, training, and model evaluation in medical VLM.

## 2. Related Work

**Vision-language models for medicine:** VQA tasks were one of the first that combined text and images directly in a single task [22]. These were later extended to FLAN-style visual instruction tuning tasks [23, 24]. General-purpose large multi-modal models such as GPT-4 [25] and Gemini [26] based on transformers [27] have demonstrated great potential towards building intelligent conversational assistants built on combined textual and vision datasets. When applied in the biomedical domain, the models present promising capabilities of understanding the basic concepts. However, handling complex domain-specific tasks with high accuracy and fine granularity remains both challenging and demanding [9, 1, 28, 3]. Pre-training and instruction tuning is important for aligning the representations across modalities and enhancing the reasoning capabilities [2, 9].

Concurrently, there have been multiple methods targeting large VLMs for medicine in different aspects. Med-Gemini [9] boasts a 1.5 Trillion parameter model and includes non-vision tasks like genomics and medical exams. LLaVa-Med [1], based on the popular LLaVa architecture [29], focused on using academic medical datasets, while Med-Flamingo [3] is an extension of Flamingo [30] that introduced a novel mechanism for combining vision and text. BiomedParse allows promptable segmentations to be performed by the VLM itself [31] but does not generalize to more com-

plex tasks like report generation. While promising first steps towards VLMs in medicine, these works highlight the limitations in precision and lack of domain expertise when applied to medical tasks, compared to traditional computer vision applications on narrow tasks such as classification and segmentation, where traditional CNNs often outperform their VLM counterparts.

### Medical vision models and expert systems:

Many models have been developed to address domain- and task-specific challenges. They achieve state-of-the-art (SOTA) performances in certain areas and often focus on expert knowledge learned from carefully curated datasets. For example, Myronenko et al. [32] created accurate lesion segmentation models for multi-modal brain MRI, He et al. [33] studied 127 common types of human anatomical structures segmentation from tens of thousands of expert annotated CT examples. Several chest X-ray classification models have been developed by Cohen et al. [34] on a wide range of publicly available datasets. Integrating domain knowledge and guided reasoning while maintaining modular flexible system design can be a plausible approach to leverage the previous successes [35, 7].

### Evaluation and benchmarking in healthcare AI:

Evaluation for vision-language models is a challenging task and is heavily dependent upon the type of task that is being evaluated. While it is straightforward to evaluate close-ended tasks such as classification, segmentation, or object detection as the well-established metrics can be directly used (e.g., F1, Dice, accuracy, etc.), it is not well-established how to evaluate more open-ended tasks where the answers have a wide range for variations. For example, open-ended questions in VQA and report generation require the evaluation of the correctness of entire sentences or paragraphs, which is challenging [36]. Many prior works attempted to evaluate the open-ended weaker VLM output by a stronger VLM. For instance, ChatGPT-4o is being used as a judge to evaluate the answer [29, 1, 37]. While using stronger VLMs as judges might be acceptable for computer vision tasks, this method of evaluation is not satisfactory for healthcare, where a factual level of precision is required, and patient outcomes depend on the results. Our evaluation shows that the capabilities of off-the-shelf VLMs like ChatGPT-4o are too limited to judge the outputs of medical VLMs directly.

**Agentic systems:** The flexibility of generative AI provides new possibilities for developing powerful medical agents that can integrate heterogeneous information and generic reasoning. Most previous works focus on extending large language models in a medical context [38, 39, 40, 41, 42]. Very recently, Hoopes et al. [43] developed a code-predicting agent framework that can integrate an array of external systems and

Table 1 | Performance of different models across various Visual Question Answering, Report Generation, and Classification benchmarks. Task-specific SOTA baselines are described in the experiments section 4.3. Datasets where \* is shown for Med-Gemini are either if a subset is used or pre-processing details have not been disclosed. (For VQARad, a particular subset was used and, pre-processing strategy for CXR dataset is undisclosed.) The highest score for each task is highlighted in bold, while the second-best is indicated with an underscore.

Model Type	Visual Question Answering			Report Generation			Classification		
Datasets	Rad MIMIC	SLAKE Path	CXR (Exp.)	CXR (Exp.)	X-ray14 (Exp.)	CheXpert (Exp.)			
Metric	Acc.	Acc.	Acc.	Acc.	BLEU-4	ROUGE	F1	F1	Tot. Avg.
Med-Gemini (1.5T)	78.8*	78.6	<u>84.8</u>	83.3	20.5*	28.3*	46.7	48.3	55.7
Task Spfc. SOTA	84.2	-	<b>86.8</b>	<u>91.7</u>	15.4	30.6	50.0	51.5	58.6
VILA-M3 (3B)	78.2	<u>82.4</u>	79.8	87.9	20.2	31.7	<u>51.3</u>	60.8	61.5
VILA-M3 (8B)	84.7	82.1	82.7	91.0	21.1	32.0	48.9	<b>61.6</b>	63.0
VILA-M3 (13B)	80.5	<b>86.4</b>	83.2	91.0	<u>21.6</u>	<u>32.1</u>	51.2	<u>61.5</u>	<u>63.4</u>
VILA-M3 (40B)	<b>90.4</b>	81.9	84.0	<b>92.7</b>	<b>21.6</b>	<b>32.2</b>	<b>51.3</b>	61.0	<b>64.3</b>

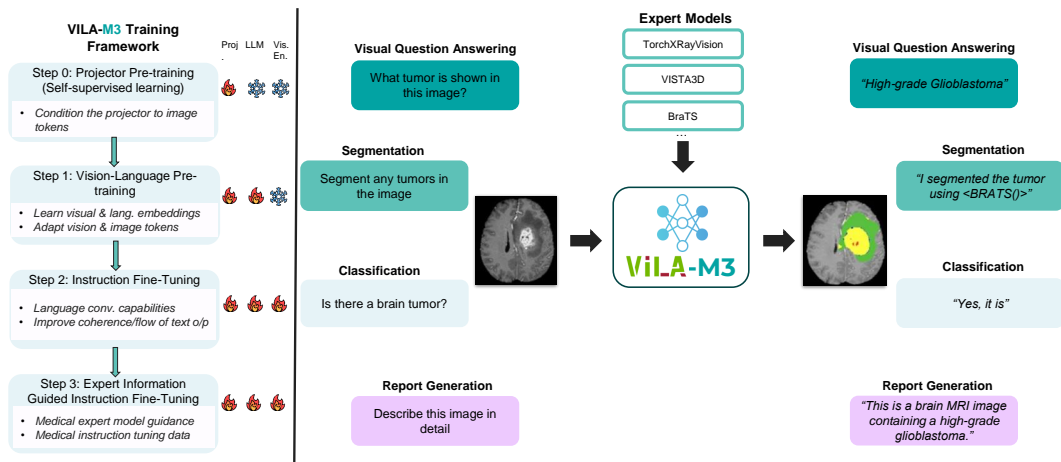


Figure 2 | VILA-M3 possesses the capability to support a diverse range of tasks, including visual question answering, classification, and report generation. Segmentation tasks are performed by suitable “expert models”, such as the BraTS brain tumor segmentation model for multimodal MRI.

APIs for a set of neuroimaging tasks including brain region analysis. Li et al. [44] proposed a multi-modal large language model invoking task-specific tools and aggregating results from them.

### 3. Method

The VILA framework [2] is suitable for pre-training vision and language models as well as instruction fine-tuning (IFT) them with domain-specific datasets. VILA-M3, in particular, leverages domain-expert model insights alongside the versatile capabilities of VILA to capture the nuances of radiological language and the intricate details of medical images, enabling more precise image-text fusion. It enhances tasks such as visual question answering (VQA), zero-shot image classification, image retrieval, and report generation, and it even incorporates expert model feedback to produce more accurate and well-reasoned outputs.

VILA is particularly applicable for medical AI, where accurate association between visual data and textual information is critical for clinical decision-making. We further enhance it by including expert model feedback that can be triggered on demand.

#### 3.1. Training Framework

The standard approach to train VLMs like VILA is to use a corpus of visual-text data where text based conversations are associated with an image. The image token is randomly inserted in between the text or before/after the text (Fig.1). As a common practice that the inclusion of text-only data is helpful towards preserving the language capabilities of VLM, we included a small corpus of medical text data [45] to specifically prevent degradation of the LLM capabilities as the model gets conditioned towards medical images.

VILA is based on auto-regressive multi-modal

LLMs, where images are tokenized into visual tokens, concatenated with text tokens, and fed into language models, effectively treating visual input as a foreign language (Fig.1). Therefore, a projector layer is needed to bridge the token embeddings from the image and text modalities. While different projector architectures are possible, a simple linear layer encourages the LLM to generalize better [2]. This approach naturally extends text-only LLMs by incorporating visual embeddings, allowing them to handle interleaved image-text inputs and generate text outputs. There are other frameworks available that combine vision and language, such as cross-attention based [3, 30], but auto-regressive approaches are gaining in popularity due to their flexibility in supporting different vision encoder and LLM backbones. Therefore, we chose VILA as it is the current SOTA for traditional computer vision and is an open-source framework. VILA models are typically trained in three training stages: projector pre-training, visual language pre-training, and IFT. VILA-M3 builds on the last stage of visual instruction tuning and expands it with the inclusion of information from domain expert models. While VILA has enough flexibility to allow for separate fine-tuning of the vision encoder, the projector, and the LLM, we fine-tune all as it is necessary to customize both vision, projector alignment, and LLM for the medical domain as shown in Fig. 2.

### 3.2. Expert Models Triggering & Feedback

In this work, we use open-source expert models for common medical imaging tasks. VILA-M3 learns to predict a keyword and argument, e.g., `<VISTA3D(hepatic tumor)>` when it wants to trigger a suitable expert model. The list of available expert models is fed as a system prompt to the model (see Fig. 2).

**Used Expert Models:** For volumetric segmentation in CT images, we utilize *VISTA3D* [33]. *VISTA3D* is a domain-specialized interactive foundation model developed for segmenting and annotating human anatomies with precision. It achieves a highly accurate segmentation of 127 classes, including challenging tumors. We include several organ or anatomy subgroups that can be chosen by VILA-M3 using different arguments when predicting the model keyword. Valid arguments are ‘everything’ (i.e., all 127 available organ classes), ‘hepatic tumor’, ‘pancreatic tumor’, ‘lung tumor’, etc. These arguments are described in model cards available to VILA-M3 as context at training and inference time (see Fig. 1). Note that when triggered, *VISTA3D* can segment the full volumetric scan even though VILA-M3 only processes 2D inputs.

For MRI imaging, we focus on tumor segmentation in multimodal brain MRI. The *MONAI BRATS*

*model* [32] consists of a pre-trained model for volumetric (3D) segmentation of brain tumor sub-regions from four MRI modalities (T1-weighted, T1-weighted with gadolinium contrast-enhancement, T2-weighted, and FLAIR) based on BraTS 2018 data and achieves good performance [46].

The majority of the data sets used for training contain chest X-rays (CXRs), which are used for many routine diagnostic clinical tasks. In this work, we utilize a model ensemble of CNN-based classification models from *TorchXRyVision* [34]. These models are trained on large cohorts of data and provide good accuracy across several diverse CXR datasets.

*Expert Model Feedback:* When VILA-M3 selects and activates an appropriate expert model from the available model cards, the result is returned to VILA-M3 as another user prompt, formatted in a conversational style. For a segmentation result, we re-tokenize the generated mask and provide a textual description that explains the significance of the segmentation results, overlaid on the original image (see Fig. 3). In the case of classification, we fed back the result as a list of yes/no statements for the likelihood that the image contains a certain disease (i.e., a list of 18 diseases using the *TorchXRyVision* ensemble).

### 3.3. Datasets

Multiple publicly available datasets were utilized for this study. We present a brief overview of them and the processing that we applied to effectively utilize them for training with the VILA framework. All training data is detailed in Supp. material.

**VQA:** In this study, we utilize the RadVQA, SLAKE, and PathVQA datasets to evaluate visual question answering (VQA) performance in medical imaging [13, 14, 15]. The SLAKE dataset comprises 642 medical images across modalities such as CXR, CT, and MRI, accompanied by 14,028 question-answer pairs covering radiology across various anatomical regions. From the official dataset splits, we used 4,919 training, 1,053 validation, and 1,061 test examples, focusing on diverse question formats like open-ended and yes/no. The PathVQA dataset includes 4,289 pathology images paired with 32,632 question-answer pairs, divided into 19,654 for training, 6,259 for validation, and 6,719 for testing. Both datasets probe a wide range of visual and clinical attributes, including abnormalities, organ identification, and diagnostic information. Our analysis focuses on using these datasets to enhance the performance of medical vision language models. We utilized both the training and validation sets from all the VQA datasets as part of the model training, due to the huge compute cost of training VLM’s standard validation techniques

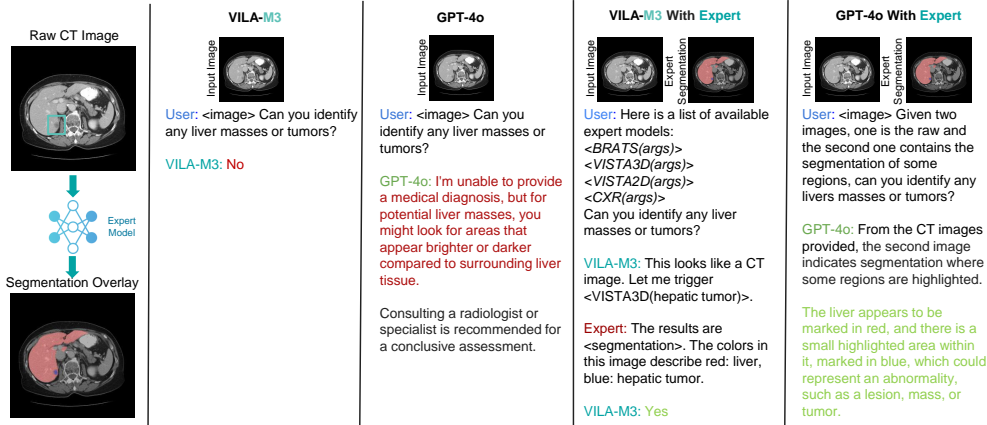


Figure 3 | Feedback of segmentation results can improve the quality of responses received from VLMs. This observation holds true for both VILA-M3 and GPT-4o. The models without expert segmentation fail to detect the tumor, unlike the models with access to expert model segmentation. The blue annotation box shows the marked tumor location, traditional VLM’s cannot capture such fine features unless guided by expert outcomes.

are quite compute heavy and also redundant.

**Classification:** We adopted two publicly available high-quality datasets of abnormalities in CXR images as a benchmark for the model’s visual classification capability. One is the subset of ChestX-ray14 [12] curated by Majkowska and Mittal et al. [47], consisted of 1,962 images after an adjudication process of four radiologists. For this dataset, we follow [9] and focus on the classification of three conditions – lung opacity, pneumothorax, and fracture. The other dataset is a subset of CheXpert [11] created by Saporta et al. [48] on the labeling of five pathological conditions, namely atelectasis, cardiomegaly, consolidation, edema, and pleural effusion.

**Report Generation:** For report generation, we adopt the MIMIC-CXR<sup>1</sup> dataset [49, 50], which provides over 377,110 CXR images in JPG format, along with structured labels extracted from 227,827 associated free-text radiology reports. Each image is linked to the corresponding radiology report, which contains the radiologists’ findings and impressions. Labels for the dataset were derived using automated tools CheXpert [11] and NegBio [51], which extract and classify medical conditions (e.g., “pneumonia,” “edema,” “pleural effusion”) as positive, negative, uncertain, or not mentioned based on the language of the reports. Additionally, radiologists manually annotate a portion of the report, providing 14 categories of findings for model evaluation and validation. The dataset is divided into training, validation, and testing parts, each with separate CSV files to support reproducible research. Due to suboptimal report quality in the initial datasets, we applied advanced Large Language Models (LLMs) to refine text reports through targeted noise reduction and finding extraction. This process significantly improved model

accuracy and reliability. Additional methodological details are available in the supplementary materials.

**Expert Datasets:** To create training data that triggers expert models for tasks like segmentation and classification, we leverage existing datasets by running expert model inference. For instance, we can segment existing CT datasets with the VISTA3D model, using the inference results to build training conversations tailored for VILA-M3. Similarly, with a brain MRI dataset, we can run the BRATS segmentation model and then utilize the output to generate structured training conversations for training VILA-M3. This approach facilitates the generation of context-specific dialogues that enhance model alignment with expert-level tasks for medical imaging. Further, we extend a subset of the existing VQA and report generation tasks by adding the model cards to the message context and adding trigger statements for the corresponding CXR expert model as illustrated in Fig. 1.

## 4. Experiments & Results

### 4.1. Model Architecture Hyper-parameters

We use the image resolution in the visual encoder at  $384 \times 384$  using OpenAI’s CLIP-L, enabling the model to capture more fine-grained visual details. For the LLM backbones, we use Vicuna (based on Llama-2 [52]) for 3 Billion and 13 Billion parameter checkpoints, for 8 Billion, we utilize Llama-3 [53] as the backbone and the 40 Billion uses Yi-34B as the LLM backbone based on Yi [54] and uses a  $448 \times 448$  vision encoder. The LLM choices depend on the configurations used for the VILA checkpoints pre-trained on natural images.

<sup>1</sup>v2.1.0

## 4.2. Implementation Details

**Training Hyper-parameters:** To ensure a fair comparison for all VILA model size variants, we kept the same training hyper-parameters for each size. A consistent batch size of 16 was maintained at the device (per GPU) level for training and 4 for evaluation. Gradient accumulation was adjusted accordingly to ensure the same overall effective batch size in multi-node training. The learning rate was initialized at  $2e-5$ , using a cosine learning rate schedule with a warm-up ratio of 0.03. Weight decay was set to zero to avoid over-regularization, and all the models utilized bf16 mixed precision, allowing efficient training with a reduced memory footprint. Gradient check-pointing was enabled to further optimize memory usage. The LLM backbone, projector, and vision encoder were kept unfrozen as that is the best setting to adapt for new data as per [2] to fine-tune the entire model.

**Training Cost:** To train these models we used A100’s with 80GB of memory. For the 3, 8, and 13 billion parameter models, we utilized four nodes (x8 A100) in parallel using 32 GPUs in total. For the 40B model, we utilized sixteen nodes, utilizing a total of 128 GPUs in parallel (Table 2). More information regarding inference computational cost can be found in the supplementary material.

**Inference Cost:** With the open source release<sup>2</sup> the computational footprints are as follows: The CXR expert dynamically loads various TorchXrayVision models and performs ensemble predictions. The memory requirement is circa 1.5GB in total. The VISTA3D expert model dynamically loads the VISTA3D model to segment a 3D-CT volume. The memory requirement is roughly 12GB, and peak memory usage can be higher, depending on the input size of the 3D volume.

Table 2 | Training computational costs for different model sizes.

#Params	Nodes	Tot. GPUs	Epochs	Train Time
VILA-M3-3B	4	32	2	~ 5.5 hrs
VILA-M3-8B	4	32	2	~ 11.0 hrs
VILA-M3-13B	4	32	2	~ 19.5 hrs
VILA-M3-40B	16	128	2	~21 hrs

## 4.3. Benchmarking

**Evaluation Metrics:** Accuracy as a measure was used to gauge the performance of close-ended questions for VQA tasks. F1-score was utilized for classification tasks. For report generation, we utilize three different metrics: BLEU-4, ROUGE, and GREEN score, which aims to be a more clinically relevant measure [57]. In

general, report generation is more challenging to evaluate and the metrics present different perspectives to understand the performance in a comprehensive manner.

**VILA-M3 Outperforms SOTA:** As a baseline comparison, we use the results from the Med-Gemini work directly [9] and task-specific SOTA baselines [1, 56, 55, 34]. Overall, the results observed in Fig. 1 indicate superior performance to existing SOTA methods that are available from either open-source or closed-source. In particular, it can be seen that markedly higher performance can be achieved in 7 out of 8 metrics with much smaller models (a few billion parameters) compared to Med-Gemini, which contains 1.5 trillion parameters on this medical benchmark.

Three models per parameter size variant were trained for 1, 2, and 3 epochs, respectively. The best performing VILA-M3 model was determined via comparison of all parameter size variants observed in Table. 1.

**VILA-M3 Benchmark:** We also evaluated VILA-M3 models on the VILA benchmark to ensure that they are not overfitting and degrading their baseline capabilities. Table. 3 summarizes the results on the base VILA checkpoint and the VILA-M3 checkpoints after expert-guided IFT.

## 4.4. Effectiveness of Expert-guided IFT

Three key results prove the effectiveness of expert-guided IFT. The first is the observation that VILA-M3 outperforms SOTA models (Fig.1 & Table.1). The second major observation is that the degradation on the VILA benchmark is not significant, after extensive training with expert-guided IFT, the performance of VILA-M3 only degrades by 7%, 11% and 4% for the 3B, 8B and 13B model variants (Table. 3). Contrastingly, the 40B model degrades by 23%, we attribute this to Llama models being superior than Yi [54] models. The third observation can be drawn that VILA-M3 is not over-fitting to the expert IFT training process for epoch 1 and 2 models. This can be visually observed in Fig. 11 that over-fitting happens for epoch 3 models, these results are shown for the 8B model (results for more model variants are available in supplementary material).

## 4.5. Ablation Studies

**Expert Model Effect:** To validate the findings of domain-expert models, we conduct experiments with VILA-M3 using the same training setting as outlined above in section 4.2. In particular, for the classification with and without expert feedback, we use the baselines of TorchXrayVision [34] and also compare it with the flagship model GPT-4o [25, 58] from OpenAI for both datasets ChestX-ray-14 and CheXpert, see Tables 5 and 6.

<sup>2</sup>Github <https://github.com/Project-MONAI/VLM>

Table 3 | Performance comparison of VILA-M3 and VILA-1.5 models across traditional vision language model benchmarks. VQAv2 is testdev split and VizWiz is test split. Avg is calculated by averaging all the benchmark scores (note that MME is divided by 20).

Model	LLM	Params	VQAv2	GQA	VizWiz	SQA-I	VQA-T	POPE	MME	MMB	MMB-CN	SEED	MM-Vet	Avg
VILA1.5	Sheared LLaMa	3B	80.4	61.5	53.5	69.0	60.4	85.9	1442.4	63.4	52.7	60.9	35.4	63.2
VILA-M3	Sheared LLaMa	3B	73.9	56.0	38.4	49.5	53.3	84.0	1381.0	60.6	51.5	59.2	23.5	56.2
VILA1.5	Llama-3	8B	83.0	63.5	63.2	82.0	68.5	85.6	1634.9	75.3	69.9	66.4	43.2	71.1
VILA-M3	Llama-3	8B	70.4	53.2	38.4	72.3	51.2	80.8	1530.0	68.8	63.3	63.1	28.2	60.5
VILA1.5	Vicuna-V1	13B	82.8	64.3	62.6	80.1	65.0	86.3	1569.5	74.9	66.3	65.1	44.3	70.0
VILA-M3	Vicuna-V1	13B	78.4	61.2	55.9	74.1	60.2	83.7	1531.0	71.3	65.5	64.8	36.6	66.2
VILA1.5	Yi-34B	40B	84.3	64.6	62.2	87.2	73.6	87.3	1726.8	82.4	80.2	69.1	53.0	75.5
VILA-M3	Yi-34B	40B	70.2	50.7	41.3	0.0	53.0	82.9	1548.5	58.9	55.6	56.8	27.4	52.2

Table 4 | Performance comparison of various models on report generation utilizing the test set from the MIMIC-CXR-JPG Database [49, 50].

Model		MIMIC-CXR w/o Expert			MIMIC-CXR with Expert		
Type	Params	BLEU-4 (↑)	ROUGE (↑)	GREEN (↑)	BLEU-4 (↑)	ROUGE (↑)	GREEN (↑)
Med-Gemini [9]	1.5T	20.5	28.3	-	20.5	28.3	-
Llava-Med [1]	7B	1.0	13.3	-	1.0	13.3	-
Llava-Rad [55]	7B	15.4	30.6	-	15.4	30.6	-
DCL [56]	0.25B	10.9	28.4	-	10.9	28.4	-
VILA-M3-3B	3B	19.7	31.4	39.4	20.2	31.7	39.1
VILA-M3-8B	8B	21.4	32.2	39.8	21.2	32.1	39.7
VILA-M3-13B	13B	21.4	32.1	39.3	21.6	32.1	39.3
VILA-M3-40B	40B	<b>21.6</b>	<b>32.2</b>	39.2	<b>21.6</b>	<b>32.2</b>	39.2

Table 5 | Performance comparison of different models on ChestX-ray14 classification tasks, both with and without expert models.

Model		ChestX-ray14 Classif. w/o Expert			ChestX-ray14 Classif. With Expert			Average	
Type	# Params	Fracture	Pneumothorax	Lung opacity	Fracture	Pneumothorax	Lung opacity	w/o Expert	Expert
GPT-4o	Unknown	2.0	19.7	77.8	-	-	-	33.1	-
Med-Gemini	1.5T	5.5	55.3	79.9	-	-	-	46.9	-
TorchXrayVision	(ensemble)	-	-	-	11.6	50.4	87.9	-	50.0
VILA-M3-3B	3B	7.0	54.5	83.8	10.8	55.2	88.1	48.4	<b>51.3</b>
VILA-M3-8B	8B	2.7	49.9	85.0	14.4	53.5	84.3	45.8	<b>50.8</b>
VILA-M3-13B	13B	7.6	55.9	86.2	13.6	51.5	88.5	49.9	<b>51.2</b>
VILA-M3-40B	40B	0.0	55.9	85.3	11.0	53.9	89.0	47.1	<b>51.3</b>

Table 6 | Performance comparison of VILA-M3 models on CheXpert classification tasks, with and without expert models.

Model		CheXpert Classif. w/o Expert					CheXpert Classif. With Expert					Average	
Type	# Params	Atel.	Cardio.	Consol.	Edema	Pl.Eff.	Atel.	Cardio.	Consol.	Edema	Pl.Eff.	w/o Expert	Expert
GPT-4o	Unknown	31.8	49.6	13.8	37.2	36.8	-	-	-	-	-	33.9	-
Med-Gemini	1.5T	49.7	72.0	23.0	32.7	64.4	-	-	-	-	-	48.4	-
TorchXrayVision	(ensemble)	-	-	-	-	-	61.5	63.8	28.6	50.5	52.9	-	51.5
VILA-M3-3B	3B	59.0	69.3	24.0	71.8	62.9	61.2	71.5	35.0	63.7	72.4	57.4	<b>60.7</b>
VILA-M3-8B	8B	63.5	63.2	35.1	73.1	71.9	62.7	70.6	36.7	68.0	64.5	61.4	<b>60.5</b>
VILA-M3-13B	13B	61.9	71.1	20.5	65.4	60.2	62.8	76.0	39.4	67.1	62.5	55.8	<b>61.5</b>
VILA-M3-40B	40B	57.2	70.4	32.6	68.3	68.7	63.4	72.1	38.4	63.7	67.4	59.4	<b>61.0</b>

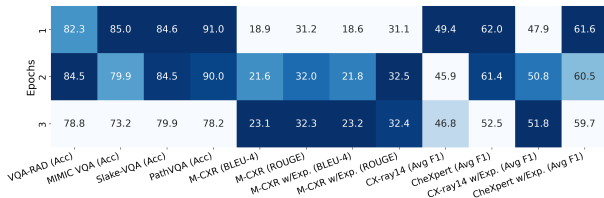


Figure 4 | The heatmap shows the performance of the 8B model on all datasets with trained models at 1, 2, and 3 epochs. It can be observed that model performance degrades for the epoch 3 model.

Experiments were performed for report generation with and without expert information inclusion

(Table 4). For comparison, we also utilize established baselines for the task-specific state-of-the-art (SOTA) ‘‘Dynamic Graph Enhanced Contrastive Learning’’ (DCL) model [56]. Notably, other baseline models considered in the study included Llama-Med [1], Llama-Rad [55], and Med-Gemini [9], in addition to the DCL models [56].

For both classification and report generation tasks, the improvements achieved by inclusion of expert models can be observed in Tables 4, 5 & 6. It can also be observed that large dataset models such as GPT-4o do not perform well on these tasks.

For segmentation tasks, observing Fig. 3 reveals that our model VILA-M3 fails to pick up on tumor



findings if segmentation is not provided. However, with additional expert information included it is able to detect the finer features of a tumor.

**Balanced vs. Unbalanced Datasets:** The original size of datasets varies a lot, especially when the original numbers are compared between VQA datasets and MIMIC-CXR. Therefore, we increased the frequency of low-count datasets in a category-wise manner (based on VQA, expert, report gen., and classification type) to systematically balance the training dataset. The training settings were kept the same as outlined in section 4.2. The training dataset table with frequency counts can be found in the supplementary materials.

The improvements based on the balanced training dataset as compared to the unbalanced dataset (original dataset size) can be observed in Fig. 5. Quantitatively, an average improvement of  $\sim 4\%$  of all metrics is gained by balancing.

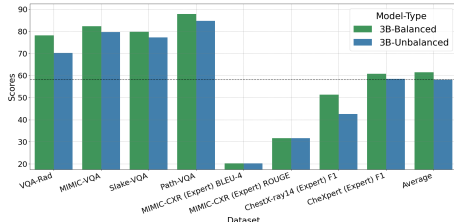


Figure 5 | Comparison of VILA-M3 training with balanced and unbalanced healthcare datasets. Comparison for 3B model is shown with a training of two epochs each.

#### 4.6. Training Convergence

Despite different model architectures and sizes, we observe that the proposed training procedures converge successfully in all cases and are not sensitive to the choice of hyper-parameters. Taking the models trained with 4 nodes (32 GPUs) as an example, Fig. 6 shows that given the same training dataset, the training loss scales with model size as expected according to the empirical power law [59].

## 5. Discussion & Conclusion

The proposed VILA-M3 model represents a significant advancement in multimodal machine learning for healthcare. It achieves SOTA performance as both a generalist model and one incorporating expert model responses to solve complex tasks. This capability allows the model to maintain high levels of performance when addressing general tasks while also leveraging expert knowledge to improve accuracy. With additional expert models, it can be seamlessly extended

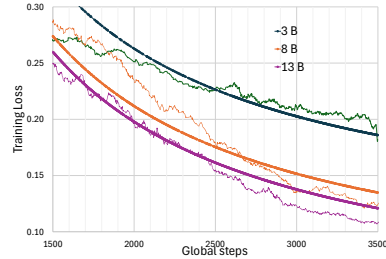


Figure 6 | Comparison of training losses at different training steps for each model after an initial transient period.

to various capabilities, such as registration, regression, etc. Our work can be seen as a step towards enabling “chain of thought” capabilities in VLMs by letting the model reason about when to trigger an expert and how to incorporate its result in the final generated prediction. For future work, we will explore the integration of Retrieval-Augmented Generation (RAG) to further enhance VILA-M3 by retrieving and incorporating relevant information from large datasets dynamically during inference. Additionally, we aim to expand VILA-M3 towards a multi-agent framework that directly incorporates smart expert models that can themselves decide whether to involve additional experts for consultation [60] to optimize performance across varied tasks.

In conclusion, the proposed VILA-M3 framework can be used to train SOTA models that consider expert model responses to improve performance on particular tasks while simultaneously exhibiting good generalist performance.

## References

- [1] Chunyuan Li, Cliff Wong, Sheng Zhang, Naoto Usuyama, Haotian Liu, Jianwei Yang, Tristan Naumann, Hoifung Poon, and Jianfeng Gao. LLaVA-Med: Training a large language-and-vision assistant for biomedicine in one day. *Advances in Neural Information Processing Systems*, 36, 2024.
- [2] Ji Lin, Hongxu Yin, Wei Ping, Pavlo Molchanov, Mohammad Shoeybi, and Song Han. Vila: On pre-training for visual language models. In *Proceedings of the IEEE/CVF Conference on Computer Vision and Pattern Recognition*, pages 26689–26699, 2024.
- [3] Michael Moor, Qian Huang, Shirley Wu, Michihiro Yasunaga, Yash Dalmia, Jure Leskovec, Cyril Zakka, Eduardo Pontes Reis, and Pranav Rajpurkar. Med-flamingo: a multimodal medical few-shot learner. In *Machine Learning for Health (ML4H)*, pages 353–367. PMLR, 2023.
- [4] Ekin Tiu, Ellie Talius, Pujan Patel, Curtis P Langlotz, Andrew Y Ng, and Pranav Rajpurkar. Expert-level

- detection of pathologies from unannotated chest x-ray images via self-supervised learning. *Nature Biomedical Engineering*, 6(12):1399–1406, 2022.
- [5] Rajesh Bhayana, Satheesh Krishna, and Robert R Bleakney. Performance of chatgpt on a radiology board-style examination: insights into current strengths and limitations. *Radiology*, 307(5):e230582, 2023.
- [6] Nolan Hayden, Spencer Gilbert, Laila M Poisson, Brent Griffith, and Chad Klochko. Performance of gpt-4 with vision on text-and image-based acr diagnostic radiology in-training examination questions. *Radiology*, 312(3):e240153, 2024.
- [7] Hareem Nisar, Syed Muhammad Anwar, Zhifan Jiang, Abhijeet Parida, Ramon Sanchez-Jacob, Vishwesh Nath, Holger R Roth, and Marius George Linguraru. D-rax: Domain-specific radiologic assistant leveraging multi-modal data and expert model predictions. In *International Workshop on Foundation Models for General Medical AI*, pages 91–102. Springer, 2024.
- [8] Andrea Cozzi, Katja Pinker, Andri Hidber, Tianyu Zhang, Luca Bonomo, Roberto Lo Gullo, Blake Christianson, Marco Curti, Stefania Rizzo, Filippo Del Grande, et al. Bi-rads category assignments by gpt-3.5, gpt-4, and google bard: A multilanguage study. *Radiology*, 311(1):e232133, 2024.
- [9] Lin Yang, Shawn Xu, Andrew Selligren, Timo Kohlberger, Yuchen Zhou, Ira Ktena, Atilla Kiraly, Faruk Ahmed, Farhad Hormozdiari, Tiam Jaroensri, et al. Advancing multimodal medical capabilities of Gemini. *arXiv preprint arXiv:2405.03162*, 2024.
- [10] Johann Li, Guangming Zhu, Cong Hua, Mingtao Feng, Basheer Bennamoun, Ping Li, Xiaoyuan Lu, Juan Song, Peiyi Shen, Xu Xu, et al. A systematic collection of medical image datasets for deep learning. *ACM Computing Surveys*, 56(5):1–51, 2023.
- [11] Jeremy Irvin, Pranav Rajpurkar, Michael Ko, Yifan Yu, Silvana Ciurea-Ilcus, Chris Chute, Henrik Marklund, Behzad Haghgoo, Robyn Ball, Katie Shpanskaya, et al. Chexpert: A large chest radiograph dataset with uncertainty labels and expert comparison. In *AAAI*, volume 33, pages 590–597, 2019.
- [12] Xiaosong Wang, Yifan Peng, Le Lu, Zhiyong Lu, Mohammadhadi Bagheri, and Ronald Summers. Chestx-ray8: Hospital-scale chest x-ray database and benchmarks on weakly-supervised classification and localization of common thorax diseases. In *CVPR*, pages 3462–3471, 2017.
- [13] Xuehai He, Yichen Zhang, Luntian Mou, Eric Xing, and Pengtao Xie. Pathvqa: 30000+ questions for medical visual question answering. *arXiv preprint arXiv:2003.10286*, 2020.
- [14] Bo Liu, Li-Ming Zhan, Li Xu, Lin Ma, Yan Yang, and Xiao-Ming Wu. Slake: A semantically-labeled knowledge-enhanced dataset for medical visual question answering. In *2021 IEEE 18th International Symposium on Biomedical Imaging (ISBI)*, pages 1650–1654. IEEE, 2021.
- [15] Jason J Lau, Soumya Gayen, Asma Ben Abacha, and Dina Demner-Fushman. A dataset of clinically generated visual questions and answers about radiology images. *Scientific data*, 5(1):1–10, 2018.
- [16] Mina Ghaffari, Arcot Sowmya, and Ruth Oliver. Automated brain tumor segmentation using multimodal brain scans: a survey based on models submitted to the brats 2012–2018 challenges. *IEEE reviews in biomedical engineering*, 13:156–168, 2019.
- [17] Seongsu Bae, Daeun Kyung, Jaehee Ryu, Eunbyeol Cho, Gyubok Lee, Sunjun Kweon, Jungwoo Oh, Lei Ji, Eric Chang, Tackeun Kim, et al. Mimic-ext-mimic-cxr-vqa: A complex, diverse, and large-scale visual question answering dataset for chest x-ray images. *PhysioNet*, 2024.
- [18] Yunfei Xie, Ce Zhou, Lang Gao, Juncheng Wu, Xianhang Li, Hong-Yu Zhou, Sheng Liu, Lei Xing, James Zou, Cihang Xie, et al. Medtrinity-25m: A large-scale multimodal dataset with multigranular annotations for medicine. *arXiv preprint arXiv:2408.02900*, 2024.
- [19] Jiawei Chen, Dingkan Yang, Tong Wu, Yue Jiang, Xiaolu Hou, Mingcheng Li, Shunli Wang, Dongling Xiao, Ke Li, and Lihua Zhang. Detecting and evaluating medical hallucinations in large vision language models. *arXiv preprint arXiv:2406.10185*, 2024.
- [20] Yutao Hu, Tianbin Li, Quanfeng Lu, Wenqi Shao, Junjun He, Yu Qiao, and Ping Luo. Omnimed-vqa: A new large-scale comprehensive evaluation benchmark for medical lvlm. In *Proceedings of the IEEE/CVF Conference on Computer Vision and Pattern Recognition*, pages 22170–22183, 2024.
- [21] Iryna Hartsock and Ghulam Rasool. Vision-language models for medical report generation and visual question answering: A review. *arXiv preprint arXiv:2403.02469*, 2024.
- [22] Stanislaw Antol, Aishwarya Agrawal, Jiasen Lu, Margaret Mitchell, Dhruv Batra, C Lawrence Zitnick, and Devi Parikh. Vqa: Visual question answering. In *Proceedings of the IEEE international conference on computer vision*, pages 2425–2433, 2015.
- [23] Jason Wei, Maarten Bosma, Vincent Y Zhao, Kelvin Guu, Adams Wei Yu, Brian Lester, Nan Du, Andrew M Dai, and Quoc V Le. Finetuned language models are zero-shot learners. *arXiv preprint arXiv:2109.01652*, 2021.
- [24] Zhiyang Xu, Chao Feng, Rulin Shao, Trevor Ashby, Ying Shen, Di Jin, Yu Cheng, Qifan Wang, and Lifu Huang. Vision-flan: Scaling human-labeled tasks in visual instruction tuning. *arXiv preprint arXiv:2402.11690*, 2024.

- [25] Josh Achiam, Steven Adler, Sandhini Agarwal, Lama Ahmad, Ilge Akkaya, Florencia Leoni Aleman, Diogo Almeida, Janko Altenschmidt, Sam Altman, Shyamal Anadkat, et al. GPT-4 technical report. *arXiv preprint arXiv:2303.08774*, 2023.
- [26] Gemini Team, Rohan Anil, Sebastian Borgeaud, Yonghui Wu, Jean-Baptiste Alayrac, Jiahui Yu, Radu Soricut, Johan Schalkwyk, Andrew M Dai, Anja Hauth, et al. Gemini: a family of highly capable multi-modal models. *arXiv preprint arXiv:2312.11805*, 2023.
- [27] A Vaswani. Attention is all you need. *Advances in Neural Information Processing Systems*, 2017.
- [28] Khaled Saab, Tao Tu, Wei-Hung Weng, Ryutaro Tanno, David Stutz, Ellery Wulczyn, Fan Zhang, Tim Strother, Chunjong Park, Elahe Vedadi, et al. Capabilities of Gemini models in medicine. *arXiv preprint arXiv:2404.18416*, 2024.
- [29] Haotian Liu, Chunyuan Li, Qingyang Wu, and Yong Jae Lee. Visual instruction tuning. *Advances in neural information processing systems*, 36, 2024.
- [30] Jean-Baptiste Alayrac, Jeff Donahue, Pauline Luc, Antoine Miech, Iain Barr, Yana Hasson, Karel Lenc, Arthur Mensch, Katherine Millican, Malcolm Reynolds, et al. Flamingo: a visual language model for few-shot learning. *Advances in neural information processing systems*, 35:23716–23736, 2022.
- [31] Theodore Zhao, Yu Gu, Jianwei Yang, Naoto Usuyama, Ho Hin Lee, Tristan Naumann, Jianfeng Gao, Angela Crabtree, Jacob Abel, Christine Moungh-Wen, et al. Biomedparse: a biomedical foundation model for image parsing of everything everywhere all at once. *arXiv preprint arXiv:2405.12971*, 2024.
- [32] Andriy Myronenko. 3D MRI brain tumor segmentation using autoencoder regularization. In *Brain-lesion: Glioma, Multiple Sclerosis, Stroke and Traumatic Brain Injuries: 4th International Workshop, BrainLes 2018, Held in Conjunction with MICCAI 2018, Granada, Spain, September 16, 2018, Revised Selected Papers, Part II 4*, pages 311–320. Springer, 2019.
- [33] Yufan He, Pengfei Guo, Yucheng Tang, Andriy Myronenko, Vishwesh Nath, Ziyue Xu, Dong Yang, Can Zhao, Benjamin Simon, Mason Belue, et al. VISTA3D: Versatile imaging segmentation and annotation model for 3d computed tomography. *arXiv preprint arXiv:2406.05285*, 2024.
- [34] Joseph Paul Cohen, Joseph D. Viviano, Paul Bertin, Paul Morrison, Parsa Torabian, Matteo Guarrera, Matthew P Lungren, Akshay Chaudhari, Rupert Brooks, Mohammad Hashir, and Hadrien Bertrand. TorchXRyVision: A library of chest X-ray datasets and models. In *Medical Imaging with Deep Learning*, 2022.
- [35] Lai Wei, Wenkai Wang, Xiaoyu Shen, Yu Xie, Zhihao Fan, Xiaojin Zhang, Zhongyu Wei, and Wei Chen. Mc-cot: A modular collaborative cot framework for zero-shot medical-vqa with llm and mllm integration. *arXiv preprint arXiv:2410.04521*, 2024.
- [36] Simon Ging, María A Bravo, and Thomas Brox. Open-ended vqa benchmarking of vision-language models by exploiting classification datasets and their semantic hierarchy. *arXiv preprint arXiv:2402.07270*, 2024.
- [37] Chaoyi Wu, Xiaoman Zhang, Ya Zhang, Yanfeng Wang, and Weidi Xie. Towards generalist foundation model for radiology. *arXiv preprint arXiv:2308.02463*, 2023.
- [38] Xiangru Tang, Anni Zou, Zhuosheng Zhang, Ziming Li, Yilun Zhao, Xingyao Zhang, Arman Cohan, and Mark Gerstein. Medagents: Large language models as collaborators for zero-shot medical reasoning. *arXiv preprint arXiv:2311.10537*, 2023.
- [39] Bufang Yang, Siyang Jiang, Lilin Xu, Kaiwei Liu, Hai Li, Guoliang Xing, Hongkai Chen, Xiaofan Jiang, and Zhenyu Yan. Drhouse: An llm-empowered diagnostic reasoning system through harnessing outcomes from sensor data and expert knowledge. *arXiv preprint arXiv:2405.12541*, 2024.
- [40] Samuel Schmidgall, Rojin Ziaei, Carl Harris, Eduardo Reis, Jeffrey Jopling, and Michael Moor. Agentclinic: a multimodal agent benchmark to evaluate ai in simulated clinical environments. *arXiv preprint arXiv:2405.07960*, 2024.
- [41] Junkai Li, Siyu Wang, Meng Zhang, Weitao Li, Yunghwei Lai, Xinhui Kang, Weizhi Ma, and Yang Liu. Agent hospital: A simulacrum of hospital with evolvable medical agents. *arXiv preprint arXiv:2405.02957*, 2024.
- [42] Hao Wei, Jianing Qiu, Haibao Yu, and Wu Yuan. Medco: Medical education copilots based on a multi-agent framework. *arXiv preprint arXiv:2408.12496*, 2024.
- [43] Andrew Hoopes, Victor Ion Butoi, John V Guttag, and Adrian V Dalca. Voxelprompt: A vision-language agent for grounded medical image analysis. *arXiv preprint arXiv:2410.08397*, 2024.
- [44] Binxu Li, Tiankai Yan, Yuanting Pan, Zhe Xu, Jie Luo, Ruiyang Ji, Shilong Liu, Haoyu Dong, Zihao Lin, and Yixin Wang. Mmedagent: Learning to use medical tools with multi-modal agent. *arXiv preprint arXiv:2407.02483*, 2024.
- [45] Di Jin, Eileen Pan, Nassim Oufattole, Wei-Hung Weng, Hanyi Fang, and Peter Szolovits. What disease does this patient have? a large-scale open domain question answering dataset from medical exams. *Applied Sciences*, 11(14):6421, 2021.
- [46] Bjoern H Menze, Andras Jakab, Stefan Bauer, Jayashree Kalpathy-Cramer, Keyvan Farahani, Justin Kirby, Yuliya Burren, Nicole Porz, Johannes Slotboom, Roland Wiest, et al. The multimodal brain

- tumor image segmentation benchmark (brats). *IEEE transactions on medical imaging*, 34(10):1993–2024, 2014.
- [47] Anna Majkowska, Sid Mittal, David F. Steiner, Joshua J. Reicher, Scott Mayer McKinney, Gavin E. Duggan, Krish Eswaran, Po-Hsuan Cameron Chen, Yun Liu, Sreenivasa Raju Kalidindi, Alexander Ding, Greg S. Corrado, Daniel Tse, and Shravya Shetty. Chest radiograph interpretation with deep learning models: Assessment with radiologist-adjudicated reference standards and population-adjusted evaluation. *Radiology*, 294(2):421–431, 2020.
- [48] Adriel Saporta, Xiaotong Gui, Ashwin Agrawal, Anuj Pareek, Steven QH Truong, Chanh DT Nguyen, Van-Doan Ngo, Jayne Seekins, Francis G Blankenberg, Andrew Y Ng, et al. Benchmarking saliency methods for chest X-ray interpretation. *Nature Machine Intelligence*, 4(10):867–878, 2022.
- [49] Alistair EW Johnson, Tom J Pollard, Seth J Berkowitz, Nathaniel R Greenbaum, Matthew P Lungren, Chih-ying Deng, Roger G Mark, and Steven Horng. Mimic-cxr, a de-identified publicly available database of chest radiographs with free-text reports. *Scientific data*, 6(1):317, 2019.
- [50] Alistair EW Johnson, Tom J Pollard, Nathaniel R Greenbaum, Matthew P Lungren, Chih-ying Deng, Yifan Peng, Zhiyong Lu, Roger G Mark, Seth J Berkowitz, and Steven Horng. Mimic-cxr-jpg, a large publicly available database of labeled chest radiographs. *arXiv preprint arXiv:1901.07042*, 2019.
- [51] Yifan Peng, Xiaosong Wang, Le Lu, Mohammadhadi Bagheri, Ronald Summers, and Zhiyong Lu. Negbio: a high-performance tool for negation and uncertainty detection in radiology reports. *AMIA Summits on Translational Science Proceedings*, 2018:188, 2018.
- [52] Hugo Touvron, Louis Martin, Kevin Stone, Peter Albert, Amjad Almahairi, Yasmine Babaei, Nikolay Bashlykov, Soumya Batra, Prajjwal Bhargava, Shruti Bhosale, et al. Llama 2: Open foundation and fine-tuned chat models. *arXiv preprint arXiv:2307.09288*, 2023.
- [53] Abhimanyu Dubey, Abhinav Jauhri, Abhinav Pandey, Abhishek Kadian, Ahmad Al-Dahle, Aiesha Letman, Akhil Mathur, Alan Schelten, Amy Yang, Angela Fan, et al. The llama 3 herd of models. *arXiv preprint arXiv:2407.21783*, 2024.
- [54] Alex Young, Bei Chen, Chao Li, Chengen Huang, Ge Zhang, Guanwei Zhang, Heng Li, Jiangcheng Zhu, Jianqun Chen, Jing Chang, et al. Yi: Open foundation models by 01. ai. *arXiv preprint arXiv:2403.04652*, 2024.
- [55] Juan Manuel Zambrano Chaves, Shih-Cheng Huang, Yanbo Xu, Hanwen Xu, Naoto Usuyama, Sheng Zhang, Fei Wang, Yujia Xie, Mahmoud Khademi, Ziyi Yang, et al. Towards a clinically accessible radiology foundation model: open-access and lightweight, with automated evaluation. *arXiv preprint arXiv:2403.08002*, 2024.
- [56] Mingjie Li, Bingqian Lin, Zicong Chen, Haokun Lin, Xiaodan Liang, and Xiaojun Chang. Dynamic graph enhanced contrastive learning for chest x-ray report generation. In *Proceedings of the IEEE/CVF Conference on Computer Vision and Pattern Recognition*, pages 3334–3343, 2023.
- [57] Sophie Ostmeier, Justin Xu, Zhihong Chen, Maya Varma, Louis Blankemeier, Christian Bluethgen, Arne Edward Michalson, Michael Moseley, Curtis Langlotz, Akshay S Chaudhari, et al. Green: Generative radiology report evaluation and error notation. *arXiv preprint arXiv:2405.03595*, 2024.
- [58] Aaron Hurst, Adam Lerer, Adam P Goucher, Adam Perelman, Aditya Ramesh, Aidan Clark, AJ Ostrow, Akila Welihinda, Alan Hayes, Alec Radford, et al. Gpt-4o system card. *arXiv preprint arXiv:2410.21276*, 2024.
- [59] Jared Kaplan, Sam McCandlish, Tom Henighan, Tom B Brown, Benjamin Chess, Rewon Child, Scott Gray, Alec Radford, Jeffrey Wu, and Dario Amodei. Scaling laws for neural language models. *arXiv preprint arXiv:2001.08361*, 2020.
- [60] Taicheng Guo, Xiuying Chen, Yaqi Wang, Ruidi Chang, Shichao Pei, Nitesh V Chawla, Olaf Wiest, and Xiangliang Zhang. Large language model based multi-agents: A survey of progress and challenges. *arXiv preprint arXiv:2402.01680*, 2024.

## Supplementary Material

### 6. Dataset Details

#### 6.1. Dataset Balancing

As shown by experiments in the *main* manuscript, dataset balancing is necessary to achieve the best performance when combining many datasets together (Main Manuscript, Figure 5). To balance the datasets, we categorized them into three broad categories: visual question answering (VQA), report generation, expert segmentation data, and language (see *Category*, Table. 7). For example, if the dataset counts are summed up category-wise, their ratios for the entire dataset can be estimated. The proportion of each category differs significantly between the original and balanced versions. While VQA was modestly increased (from 24.9% to 30.4%), language and expert segmentation data were substantially increased (1.2% to 5.5% and 7.9% to 34.8%, respectively), whereas report generation was decreased (33.0% to 14.7%).

Type	Dataset	Category	Original	Freq.	Balanced
Raw	USMLE	Lang	10,178	10	101,780
Raw	RadVQA	VQA	6,281	16	100,496
Raw	SLAKE	VQA	5,972	16	95,552
Raw	PathVQA	VQA	26,034	4	104,136
Expert	MIMIC-Diff-VQA	VQA	129,232	2	258,464
Expert	MIMIC	Report	270,000	1	270,000
Expert	VISTA3D	Seg	50,000	8	400,000
Expert	BRATS	Seg	15,000	16	240,000
Total			819,456		1,840,428

Table 7 | Balanced training dataset statistics showing original and balanced sample counts.

#### 6.2. Report Dataset Curation

The preparation involves downloading datasets and refining report text with a Large Language Model (LLM) to create high-quality inputs for generating reliable medical reports. The primary dataset used is the **MIMIC Chest X-ray JPG Database v2.0.0** [49, 50], which contains over 377,000 images and 227,827 free-text radiology reports. These data are de-identified to comply with HIPAA requirements. The process incorporates text enhancements and cleansing to optimize the quality of report inputs.

##### 6.2.1. Download Datasets

The process begins with downloading the MIMIC-CXR-JPG dataset, which provides chest X-ray images and corresponding radiology reports. Data splits and labels are standardized, and enhanced text versions are utilized for improved report quality. The dataset is designed for tasks involving medical image analysis and natural language processing. Enhanced text

versions ensure clarity and remove noise for better performance in model training. To refine the quality of the reports and eliminate noise, we utilize an enhanced text version developed by DCL [56], and subsequently apply additional cleansing procedures to further optimize report accuracy.

##### 6.2.2. Sentence Pool Collection

To standardize the language used in medical reports, a pool of sample sentences is created. This pool consists of commonly recurring phrases or sentence structures that appear in radiology reports. Using python scripts, the LLM (Llama-3.1-8b-instruct) analyzes the dataset and extracts these patterns, which are stored in a file (e.g., `sentence-pool.txt`) to guide the text transformation process.

##### Example: Sentence Pool:

- The cardiac silhouette is normal in size.
- The lungs are low in volume.
- No pleural effusions.
- No pulmonary edema.
- There is mild pulmonary vascular congestion.

##### Prompt Example for Collection:

"Analyze the medical report dataset and extract recurring sentence structures. Compile these into a pool of sample sentences to be used for standardizing input text."

##### 6.2.3. Text Conversion Using LLM

The LLM (Llama-3.1-8b-instruct) utilizes the sentence pool to process the text, replacing or reformatting sentences and medical terminology into a consistent and standardized format. This step ensures uniform input data for the VLM model, improving its ability to generate reliable and accurate reports.

##### Example:

- **Before Conversion:**  
"Lungs are low in volume. Congestion of the pulmonary vasculature, small bilateral pleural effusions and presence of septal lines reflect mild pulmonary edema."
- **After Conversion:**  
"The lungs are low in volume. There is mild pulmonary vascular congestion. No pleural effusions are seen."

##### Prompt Example for Conversion:

"Using the provided sentence pool, transform the medical report text into a consistent format. Ensure the output text aligns with the predefined sentence structures without altering the content's meaning. Return only the standardized text."

### 6.3. Expert Dataset Curation

**Segmentation:** For segmentation models, we can train VILA-M3 to trigger a suitable expert model together with several different input arguments. For example, when triggering the VISTA3D model, we generate several variations (using Llama-3.1) of instructions to the model to segment a certain anatomical structure in the image and give a suitable trigger message. For instance:

- User: Can you identify any liver masses or tumors?  
VILA-M3: This looks like a CT image. Let me trigger <VISTA3D(hepatic tumor)>.
- User: Can you assist me in segmenting the bony structures in this image?  
VILA-M3: I segmented the skeleton using <VISTA3D(skeleton)>.
- User: Segment the entire image.  
VILA-M3: I segmented the entire image using <VISTA3D(everything)>.

For these types of instructions, VILA-M3 predicts the suitable arguments for the VISTA3D model in order to trigger the segmentation of the correct anatomical structure as illustrated in Fig. 7. We built these types of instruction and answer pairs into the expert training dataset in order to build segmentation capabilities into VILA-M3. Table 8 summarizes the expert models and datasets used in this work to build up the expert training dataset.

Table 8 | Expert Selection Training Data.

Modality	Expert	Datasets
CT	VISTA3D	MSD (liver, spleen, pancreas), TotalSegmentatorV2
MRI	BRATS (SegResNet)	BRATS (2018)
CXR	TorchXRyVision	MIMIC (Reports, VQA)

**Report Generation:** Converting expert model predictions into conversation format involves transforming classification outputs into structured dialogues for AI training in medical report generation. Initially, ensemble predictions are created by combining probabilities of various medical conditions (like Atelectasis and Effusion) from multiple expert models from TorchXRyVision applied to chest X-ray images. These probabilities are interpreted to determine the presence ("yes") or absence ("no") of each condition based on a threshold.

The formatted expert predictions are then integrated into conversation prompts that include an image placeholder, a prompt for report generation, and the expert results as additional information. For example, the prompt might be:

```
<image>
Describe the image in detail.
When answering, please incorporate
the expert model results:
Atelectasis: yes
Cardiomegaly: no
Effusion: yes
```

Each conversation is assembled into a structured format containing a unique identifier, the image reference, and the dialogue between the human and the VLM model. This approach enriches the dataset with various prompt types and simulates interactions where the VLM model provides diagnoses based on image analysis and expert insights, enhancing the model's ability to generate accurate and contextually rich medical reports.

## 7. Training & Compute Details

### 7.1. Training Details

The loss curves for all model variants when training for 2 epochs can be observed in Fig. 8. The largest change in the training loss can be observed between 3B and 8B, 13B and 40B models. There is a significant learning gap that one can observe between 3B and 8B onwards, which demonstrates that the 3B model learning capabilities are limited. It should also be noted that the 40B model has a noisier training curve as compared to all other models, this can be attributed to two major factors, the first being that the vision backbone is much larger (6B parameters) as compared to other configurations and the second factor being that it is a Yi model [54] and their learning behavior is different. The training trends overall also indicate that larger models have diminishing returns in terms of loss convergence, note that the 8B, 13B and 40B are quite close in terms of the final loss values. The 40B model loss stays quite high during training and takes a longer time to converge below the loss values of other models, indicating that it is slower to train.

### 7.2. Inference Compute

We have successfully deployed an inference workflow of the proposed framework. While there are additional techniques (such as TensorRT) could be used to

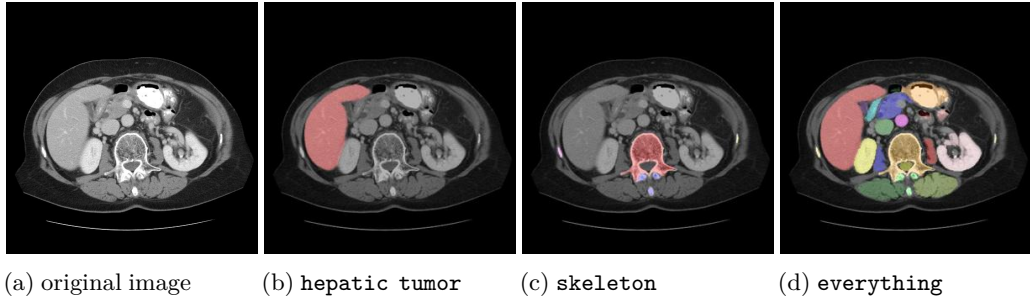


Figure 7 | (a) The original CT image slice. (b-d) The selected argument by VILA-M3 to the VISTA3D expert model call.

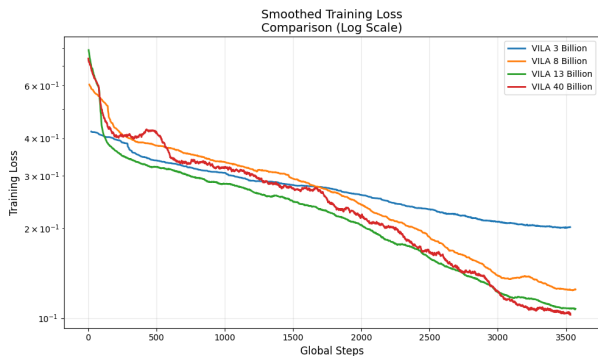


Figure 8 | Comparison of training trends across all model variants by parameter size. The compared variants are 3, 8, 13, and 40 billion parameter models.

improve the system throughput, we list the computational costs without ‘bells and whistles’ to show the technical feasibility of practical usages in Table 9.

Model		VLM Properties		
Type	# Params	VRAM (GB)	tokens/sec	Max context len
VILA-M3	3B	7	41	4,096
VILA-M3	8B	18	32	4,096
VILA-M3	13B	30	26	4,096
VILA-M3	40B	77	9	4,096

Table 9 | Inference computational costs for VILA-M3 variants.

## 8. Additional Experiments

### 8.1. Scaling Law Experiment Additional Details

Table 10 | Fits to  $L(N,S)$  of the loss scaling law defined in [25] Equation 5.6. These parameters are visualized in Main Manuscript Fig 6.

Parameter	$\alpha_N$	$\alpha_S$	$N_c$	$S_c$
Value	0.78	1.09	$1.50 \times 10^8$	$3.92 \times 10^2$

In the Main Manuscript, Fig. 6 shows that after an

initial warm-up period, the learning curve of the fine-tuning processes can be approximately fit by a universal function parameterized by model size and number of steps (using 32 GPUs in this case). Table 10 summarizes the empirical fit of the power law parameters based on Equation 5.6 in [59]. It is interesting to observe that although our fine-tuning dataset size is relatively small compared with a typical LLM training scratch setup, the training process scales according to the model size and training steps following a similar pattern.

### 8.2. Balanced & Unbalanced Datasets Training

Since the original size of datasets varies a lot as can be observed in Table. 7. In the main manuscript we showed the comparison between balanced and unbalanced datasets for the 3B model. Here, we plot additional results for the 8B and 13B models both as shown in Fig.9.

The improvements based on the balanced training dataset as compared to the unbalanced dataset (original dataset size) can be observed in Fig. 9. Quantitatively, an average improvement of  $\sim 4\%$  of all metrics is gained by data balancing for the 3B and 13B models. The 8B model shows an improvement of  $\sim 2\%$ . Furthermore, the training trends in Fig. 10 indicate that the balanced dataset provides an earlier convergence in the loss and an overall lower loss training trend is achieved.

### 8.3. Comparisons With GPT-4o For Classification

Tables 5 & 6 (Main Manuscript) show a comparison with GPT-4o [25, 58] for classification experiments. The inference on GPT-4o was performed with the same prompt as being used for VILA-M3. The images were pre-appended to the prompt via API call using a python script and then the responses were collected with retry attempts set to 10.

We often found that with API usage the GPT-4o provided inconsistent responses as it took more 3-5 retries for more than quite a few images for both CheXpert

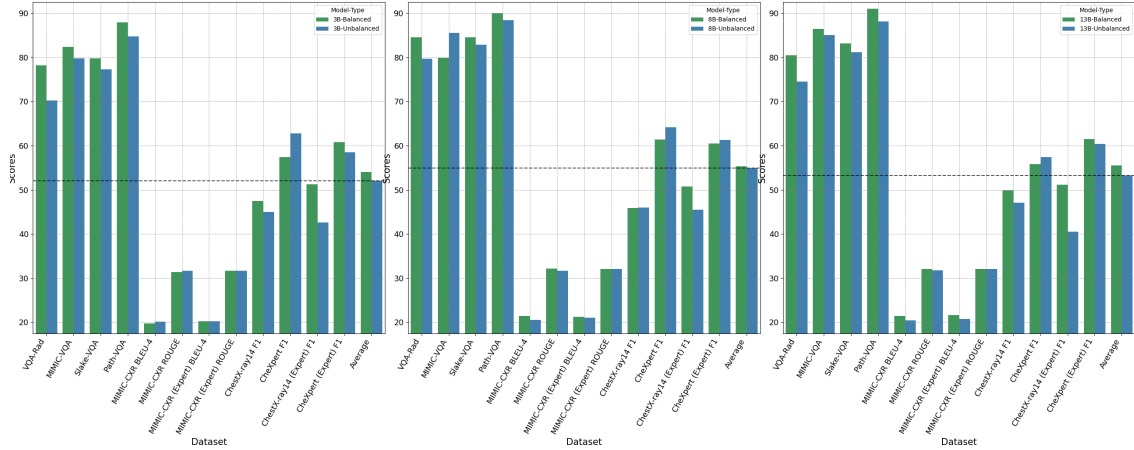


Figure 9 | Comparison of VILA-M3 training with balanced and unbalanced healthcare datasets. Comparison for 3B, 8B and 13B model are shown with a training of two epochs each

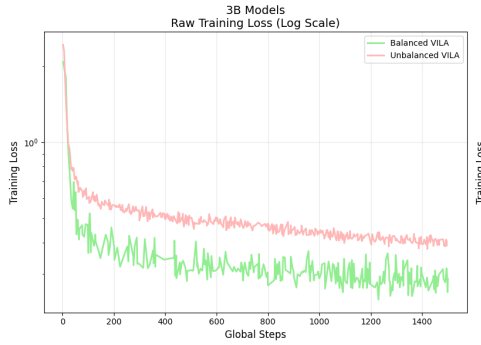


Figure 10 | Comparison of training trends across 3B model to show the effect of balanced and unbalanced dataset on model training.

and Chest X-ray datasets. We also found that if we appended the *expert model information*, the GPT-4o refused to provide responses for many images and therefore a quantitative analysis would be unfair. For more than 50% images responses could not be successfully retrieved. We believe the guardrails of GPT-4o likely come into effect when a sufficient amount of medical terminology is used within the prompt itself.

#### 8.4. Statistical significances of the classification experiments

We conduct McNemar’s Chi-square tests to show that the proposed M3 models (with expert models) significantly differ from GPT-4o (results shown in Main Manuscript Table 5 and 6). The values that are smaller than 0.05 indicate significance. For the corresponding model and specific class denoted with \*, M3 is significantly better than GPT-4o.

	Fracture	Pneumothorax	Lung opacity
M3-3B	5.5e-10*	3.2e-5*	6.1e-41*
M3-8B	1.3e-1	3.1e-1	4.5e-14*
M3-13B	5.9e-20*	5.0e-8*	1.0e-44*
M3-40B	3.1e-12*	2.5e-8*	3.2e-49*

Table 11 |  $p$ -value for the null hypothesis that the classification models perform at the same level as GPT-4o for each class on ChestXray14.

	Atel.	Cardio.	Consol.	Edema	P1. Eff.
M3-3B	2.3e-53*	2.1e-37*	6.5e-43*	7.0e-48*	2.6e-51*
M3-8B	3.7e-59*	1.0e-16*	3.4e-33*	1.3e-30*	1.3e-32*
M3-13B	2.0e-46*	2.9e-30*	4.6e-22*	1.3e-41*	1.3e-32*
M3-40B	6.6e-52*	2.5e-18*	2.8e-23*	3.2e-47*	3.8e-40*

Table 12 |  $p$ -value for the null hypothesis that the classification models perform at the same level as GPT-4o for each class on CheXpert.

#### 8.5. Additional Results Expert-Guided IFT

From the main manuscript in Fig 4. it was observed that the 8B model overfits when the 3 epoch variant is trained. In Fig. 11 results for all datasets for all model variants (3B, 8B, 13B and 40B) can be observed. The performance deterioration for all datasets is evident for the 3 epoch model for all variants with the exception of report generation tasks. Since the report generation task is of a much more complex nature the models do not overfit to it.

#### 8.6. Additional Results on Report Generation

We conducted a detailed analysis of the test set results for report generation, focusing on the disease and pattern distribution (multi-label ground truth) from the **MIMIC Chest X-ray JPG Database v2.0.0**. This evaluation utilized the best-performing 40B model, covering both with and without the integration of expert model predictions. Table 13



shows performance metrics with and without expert model predictions across various categories of medical findings. Key metrics include BLEU-4, ROUGE, and GREEN score (GREEN), evaluated for both settings. For most categories, the inclusion of expert models resulted in marginal improvements in the GREEN metric, which measures overall accuracy. For instance, in the *Atelectasis* category, GREEN improved from 35.93 to 36.56, and in *Cardiomegaly*, it increased from 38.99 to 39.79. However, some metrics, such as BLEU-4 in categories like *Fracture* and *Lung Lesion*, showed slight decreases when expert model predictions were used.

Notably, the *No Finding* category exhibited the largest improvement in green (45.60 to 46.57), indicating that expert models may be particularly effective in identifying cases with no abnormalities. These results suggest that while the integration of expert models generally enhances certain metrics, the gains are context-dependent and may vary across different medical conditions.

## 9. Additional Discussion

As also stated in the main manuscript, we will explore the integration of Retrieval-Augmented Generation (RAG) to further enhance VILA-M3 by retrieving and incorporating relevant information from large datasets dynamically during inference.

Further improvements would be to make an agentic framework with expert models, however it requires careful design. However, implementing an agentic framework necessitates careful design to balance autonomy with control, ensuring the system remains reliable and interpretable. Addressing these design challenges will be crucial for advancing the model’s capabilities and for its successful deployment in complex real-world applications.

The results of this work indicate that we need to carefully curate data and factor in expert information from the many medical domain-specialized models that have been trained in the past.

Table 13 | Detailed performance on report generation with and without expert models.

Category	Quantity	Without Expert			With Expert		
		BLEU-4 ( $\uparrow$ )	ROUGE	GREEN	BLEU-4	ROUGE	GREEN
Atelectasis	494	19.21	31.32	35.93	19.03	31.31	36.56
Cardiomegaly	426	18.62	32.11	38.99	18.38	31.98	39.79
Consolidation	99	18.46	31.47	37.23	18.20	30.70	34.97
Edema	451	20.69	33.39	38.97	20.54	33.68	39.66
Enlarged Cardiomeastinum	70	16.10	27.63	31.86	16.67	28.57	35.28
Fracture	53	19.12	31.07	37.51	17.24	30.20	35.88
Lung Lesion	83	20.75	32.92	38.89	18.64	31.56	36.17
Lung Opacity	759	18.60	30.35	35.92	17.96	30.18	35.30
No Finding	561	21.20	34.25	45.60	21.81	34.16	46.57
Pleural Effusion	678	18.52	30.60	34.53	18.20	30.44	35.12
Pleural Other	37	19.27	29.37	32.09	17.32	27.42	36.10
Pneumonia	219	19.39	32.30	38.41	20.14	32.91	39.43
Pneumothorax	58	18.76	29.97	30.02	17.39	28.62	27.71
Support Devices	635	19.25	30.70	35.24	19.19	30.42	35.91

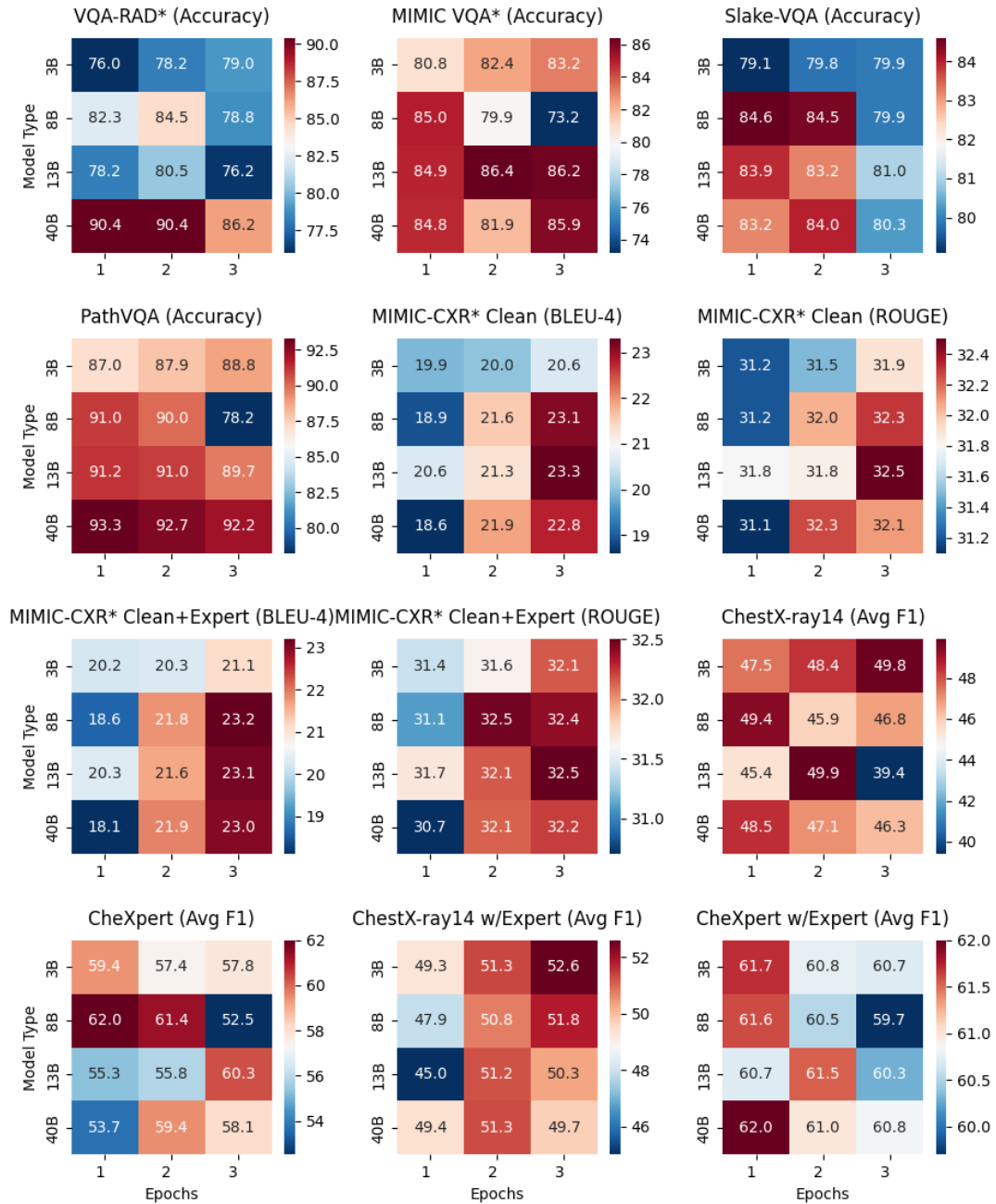


Figure 11 | The heatmap shows the performance of the all model variants 3B, 8B, 13B and 40B on all datasets with trained models at 1, 2 and 3 epochs.